Detailed Description of research work

Title: *"Overcoming Formulation Challenges of a Universal Antioxidant: Crafting Stability and Therapeutic Efficiency"*

1. Introduction

Lipoic acid (LA) is a dietary supplement with a double-sulfhydryl structure that acts as a cofactor for enzymatic complexes involved in cellular energy production [1,2]. LA is known to exhibit antioxidant and anti-inflammatory characteristics, by enhancing the functioning of antioxidant enzymes like glutathione reductase and reinstatement of the equilibrium between reduced and oxidized glutathione [3]. Inflammation and oxidative stress are common features observed in various pathological conditions like diabetic polyneuropathy and Alzheimer's disease. These conditions are characterized by the activation of inflammatory pathways, leading to an overproduction of nitric oxide (NO) and reactive oxygen species (ROS) [4]. A recent clinical study also demonstrated that a four-month treatment with LA in patients with type 2 diabetes mellitus led to significant reduction in inflammatory markers (C-reactive protein [CRP], interleukin-6 [IL-6] and tumor necrosis factor-alpha [TNF- α]) [5]. Unfortunately, this exceptional therapeutic potential of LA is limited by certain technological challenges including low aqueous solubility and susceptibility to heat-induced degradation [2].

In recent years, significant progress has been made in nanotechnology to ameliorate the effectiveness of hydrophobic compounds by leveraging their unique biological properties and adaptable structure. These advancements have resulted in the development of various nanoformulations of LA for different applications, including nanoemulsions [6], lipid nanoparticles [7], polymeric nanoparticles [8], polymer-drug conjugates [2] and self-emulsifying delivery systems (SEDS) [9]. However, till date no such formulation has the capability to take LA from bench to bed side.

Considering these limitations, current work utilized the exploration of three different novel and innovative formulation approaches: polymer-drug conjugation, cyclodextrin inclusion complexes combined with nanofiber technology, and solid dispersion techniques. The first strategy involves the synthesis of a lipoic acid-polymer conjugate *via* carbodiimide coupling to enhance its antiepileptic efficacy. In the

second approach, lipoic acid-cyclodextrin inclusion complex is formulated and encapsulated within nanofibers to develop patient-friendly, orally disintegrating delivery systems (ODDSs) without the use of toxic organic solvents. The final strategy focuses on the solid dispersion of lipoic acid to improve its therapeutic efficacy. The outcomes of this research offer promising avenues for the efficient delivery of lipoic acid, advancing its pharmacological potential from experimental settings to clinical application.

2. Objectives

- *Synthesis of tocopherol polyethylene glycol succinate (TPGS) polymer-LA conjugate to ameliorate the anti-epileptic efficacy of LA.*
- *Development of effective and patient-friendly orally disintegrating nanofiber encapsulating cyclodextrin-LA inclusion complex.*
- *Development of LA solid dispersion and evaluation of therapeutic potential in OVA-LPS induced allergic asthma in murine model.*

3. Material and Methods

3.1 Materials

D-α-Tocopherol polyethylene glycol 1000 succinate (TPGS), pentylenetetrazol (PTZ), anhydrous dichloromethane (DCM), 4-(dimethylamino) pyridine (DMAP), a Pur-A-Lyzer dialysis kit (MWCO 1 kDa), Hydroxypropyl-β-cyclodextrin (HP-β-CD) and TRIZOL reagent were purchased from Sigma-Aldrich. (R)-α-Lipoic acid (LA) and Pullulan (PUL) were purchased from Tokyo Chemical Industry (TCI). 1-ethyl N-3-(3-(dimethylamino)propyl) carbodiimide hydrochloric acid (EDC·HCl) was procured from HiMedia Laboratories. A Verso cDNA synthesis kit and GoTaq qPCR Master Mix were procured from Thermo Fisher Scientific and Promega, respectively. All other solvents and reagents used were of analytical grade

3.2 Synthesis and Characterization of TPGS-(R)-α-Lipoic Acid Conjugate (TPGS-LA).

TPGS-Lipoic acid (TPGS-LA) conjugate was synthesized via a single-step carbodiimide acid−alcohol coupling reaction by using EDC·HCl as a coupling agent and DMAP as a base (Scheme 1) [10, 11]. The resultant product was dried under reduced pressure, dissolved in ethanol, and dialyzed (via a Pur-A-Lyzer

dialysis kit, MWCO 1 kDa) in two steps for 72 h, first against 70 % ethanol for 24 h and then against deionized water for 48 h to remove unreacted LA and side products. The purified product was lyophilized (Labconco FreeZone freeze-dryer) and stored at −20 °C for further use. The conjugation of LA with TPGS was analyzed using NMR, FT-IR, and MALDI. ^{1}H NMR (600 MHz) and ^{13}C NMR (151 MHz) spectra were recorded for LA, TPGS, and TPGS-LA conjugate by an NMR spectrometer (AV-600, Bruker) using $CDCl_3$ as the solvent. The FT-IR spectra were recorded using a PerkinElmer FT-IR spectrometer in chloroform over the range 4000−500 cm^{-1}. UV spectra of synthesized TPGS-LA conjugate was also analyzed using a GENESYS 180 UV− vis spectrophotometer.

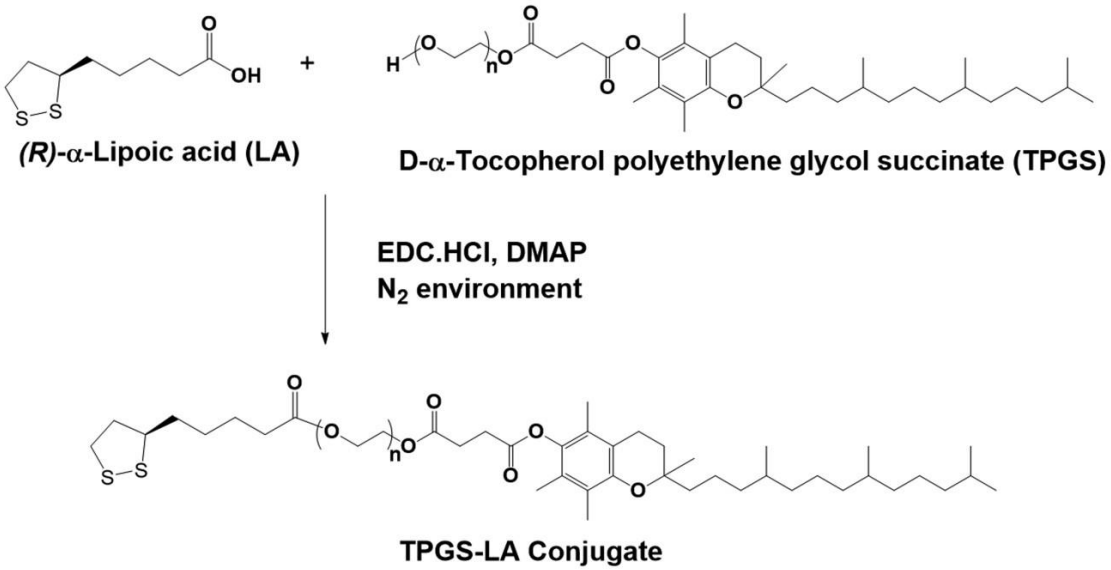

Scheme 1: Synthetic scheme for D-α-tocopherol polyethylene glycol succinate 1000 (TPGS)-lipoic acid (TPGS-LA) conjugate. EDC·HCl: 1-Ethyl N-3-(3-(dimethylamino)propyl)) carbodiimide hydrochloric acid. DMAP: 4-(Dimethylamino) pyridine.

3.3 Development and characterization of lipoic acid/cyclodextrin inclusion complex pullulan nanofiber

The IC of LA with M-*β*-CD (selected based on phase solubility studies) was prepared by mixing them in 1:1 M stoichiometric ratio (LA: M-β-CD). Initially, M-*β*-CD (23 % w/v) was dissolved in water followed by the addition of LA [12]. The mixture was incubated overnight at room temperature (RT) with continuous stirring, resulting in a clear solution of the inclusion complex. Further, PUL (20 % w/v) was incorporated in the LA-M-β-CD IC solution and stirred at RT to get clear

solution. The conductivity and viscosity of the solution was also measured using a conductivity meter (deluxe conductivity meter, Model-602) and viscometer (IKA ROTAVISC lo-vi), respectively. The developed solution was filled in 1 mL syringe with stainless-steel needle (27 G) and was subjected for electrospinning (E-SPIN NANOTECH, model: Super ES-1) at high voltage (15 kV) with constant flow rate of 0.7 mL/h [13]. The blank NF consisting of pure PUL and CD solutions without LA was also prepared using the same protocol.

Further, developed nanofiber was characterized via SEM, FTIR, DSC, TGA, XRD, *in vitro* time dependent release, dissolution and disintegration.

3.4 Development and characterization of lipoic acid solid dispersion

Solid dispersion of LA was prepared in selected polymeric carrier (Soluplus) by freeze drying method [14]. Briefly, 2 % aqueous solution of Soluplus (SOL) was prepared and mixed with ethanolic solution of lipoic acid in 1:5 ratio (LA: SOL). The resultant solution was incubated overnight with continuous stirring and frozen at -70 °C. Afterwards, the mixer was freeze dried, followed by grinding and sieving, and stored in desiccator till further use. The physical mixture of LA and SOL was simply prepared by mixing them together in ratio 1:5 using mortar and pastel. The developed solid dispersion was characterized via SEM, FTIR, XRD, DSC and *in vitro* dissolution.

3.5 Evaluation of ameliorated therapeutic efficacy of developed LA conjugate, nanofiber and solid dispersion

3.5.1 *Evaluation of Biocompatibility and anti-epileptic efficacy of TPGS-LA on Zebrafish model*

The biocompatibility of synthesized TPGS-LA conjugate was investigated by analyzing the complete embryonal development of zebrafish embryos up to 120 h postfertilization (hpf). The PTZ drug, a common chemo□convulsant, acts as an antagonist to the γ-aminobutyric acid (GABA) receptor and induces seizures. PTZ-induced seizures in the zebrafish larvae manifest three different stages, i.e., stage I, hyperactivity stage, characterized by an increase in speed and abnormal swimming pattern; stage II, whirlpool stage exhibiting circular whirlpool-like movements; and stage III, clonus-like seizure stage with strong body twitching movements resulting in a sloping position accompanied by complete loss of

posture [15]. Concisely, 7 dpf larvae were randomly divided into four groups, LA1, LA5, LA10, and TPGS-LA, with 10 larvae in each group, and were incubated for 1 h in 1, 5, and 10 µM concentrations of LA and a 5 µM concentration (equivalent to LA) of TPGS-LA conjugate, respectively (dpf, days postfertilization). After incubation, each larva was gently transferred to the well [3.5 cm (diameter), 2 cm (depth)] containing 3.5 mL of 8 mM PTZ solution maintained at 28 ± 0.5 °C, and latency to first clonus seizures (stage III) was noted with a fixed upper cut-off timing of 15 min. Further, *c-fos* gene expression and protein carbonylation was also evaluated.

3.5.2 *In vitro* evaluation of anti-inflammatory potential of nanofibers in RAW 264.7 cells

The biocompatibility and anti-inflammatory potential of developed LA nanofibers were evaluated in RAW 264.7 cells at different concentrations. Further, effect of developed nanofibers on NO production and ROS generation was also evaluated. Finally, qRT-PCR of pro-inflammatory enzyme and cytokine genes, Western blot of primary pro-inflammatory enzyme (COX-2) and NF-κB protein translocation assay was also conducted to generate deeper mechanistic insights on anti-inflammatory effect of lipoic acid.

3.5.3 *In vivo* evaluation of ameliorated therapeutic potential of developed LA solid dispersion in OVA-LPS induced allergic asthma murine model

The amelioration in therapeutic efficacy of lipoic acid after development of solid dispersion and SEDS was evaluated in OVA-LPS induced allergic asthma murine model. In brief, for evaluation, the lung allergic inflammation was induced by OVA and LPS. The Mice were divided into 5 groups (n = 5) viz, 1. control, 2. OVA-LPS control, 3. Lipoic acid (50 mg/kg/animal), 4. LASD (50 mg/kg/animal), 5. LASEDS (50 mg/kg/animal). All groups were administered orally once a day during the study period of 28 consecutive days. At end of the study, mice were euthanized using CO_2 asphyxiation, following which blood, and lungs were collected. A part of lung tissue was stored in 10 % formalin for histological and immunohistochemical staining. The remaining tissue was homogenized and used for subsequent evaluation of numerous biochemical assays, gene and protein expression and activation.

3.6 Statistical analysis

The results were displayed as the mean and standard deviation (SD) for three separate values (n = 3). One-way analysis of variance with a Tukey's post hoc test was used to determine the significant difference between the means of each group using the graph pad prism software 9 (GraphPad Software Inc., CA, USA) at significance level of $p < 0.05$.

4. Results and Discussion

4.1 Synthesis, Characterization and ameliorated anti-epileptic efficacy of TPGS-(R)-α-Lipoic Acid Conjugate (TPGS-LA) evaluated in zebrafish model

In this strategy, we have explored the polymer drug conjugation approach to augment the therapeutic efficacy of α-lipoic acid. TPGS-LA conjugate was synthesized via esterification between the carboxylic acid group of LA with the hydroxyl group of TPGS. Excessive LA was used in order to achieve a complete reaction as it is easier to separate the low-molecular-weight LA from the large molecular TPGS-LA conjugate. The synthesized TPGS-LA conjugate was confirmed by ^{1}H and ^{13}C NMR spectroscopy (Figure 1 a,b). The ^{1}H NMR spectrum of TPGS demonstrated characteristic peaks of methylene protons in vitamin E at δ 0.86 ppm and CH_2-CH_2-O- (PEG chain) protons at δ 3.6 ppm (Figure 1a) [16,17]. Similar peaks were observed in the 1 H NMR spectrum of TPGS-LA conjugate along with peaks corresponding to LA at δ 3.11−3.18 ppm, thus confirming the successful reaction between TPGS and LA.27 Further, ^{13}C NMR of TPGS-LA conjugate shows the peaks of both LA and TPGS (Figure 1b). The spectrum of TPGS demonstrated peaks at δ 171 and δ 172 ppm corresponding to its two carbonyl (-C-O) groups. The peak in the ^{13}C NMR results at δ 180 ppm (because of the carboxylic group of LA) was shifted upfield to δ 173 ppm in TPGS-LA conjugate due to ester bond formation, and a total of three peaks at the δ 171, δ 172, and δ 173 ppm region were observed, representing three carbonyl groups (two of TPGS and one of LA) [18].

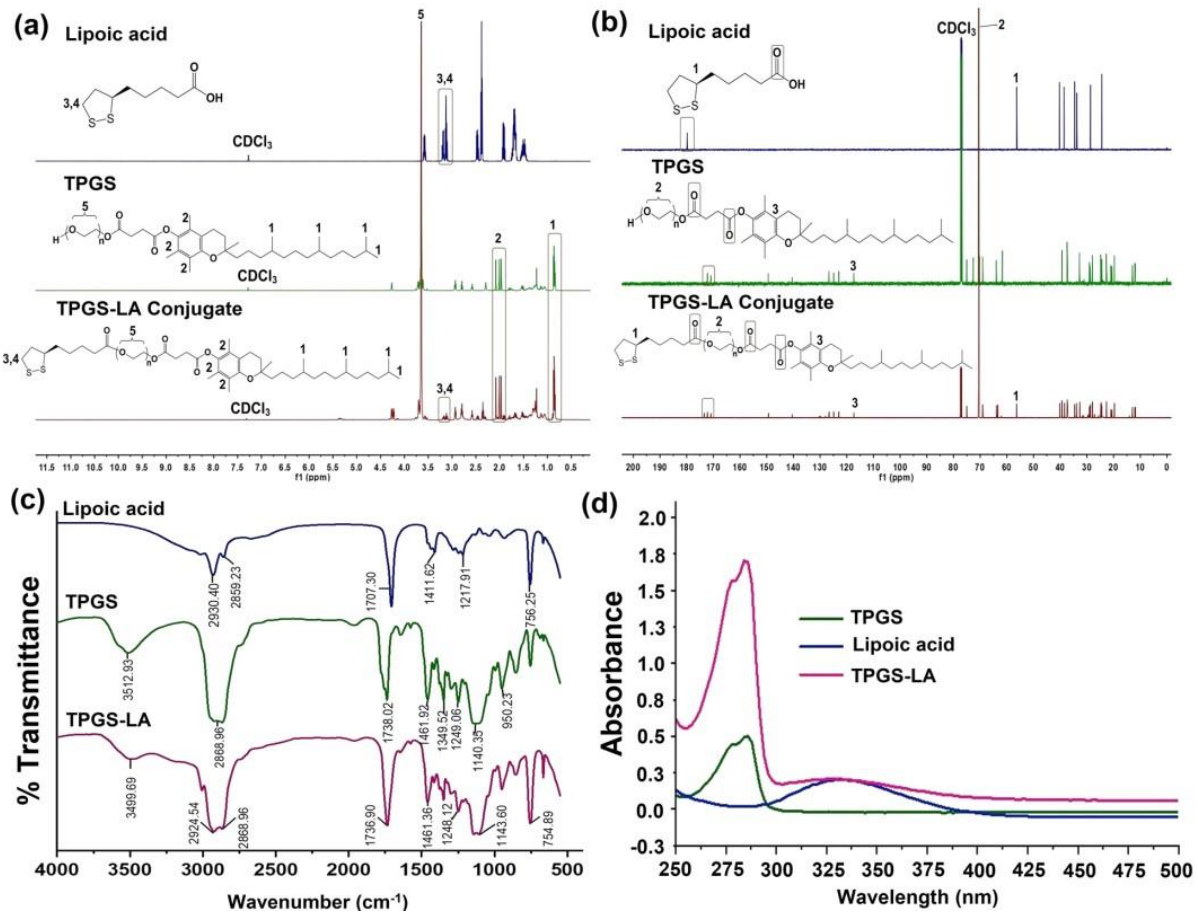

Figure 1: (a) ^{1}H (600 MHz) and (b) ^{13}C NMR (151 MHz) spectra of native lipoic acid (LA), TPGS, and TPGS-LA conjugate in deuterated chloroform ($CDCl_3$). The NMR spectrum of TPGS-LA conjugate demonstrated peaks of both TPGS and LA. The peak in the 13C NMR at δ 180 ppm (due to the carboxylic group of lipoic acid) was shifted upfield to δ 173 ppm in TPGS-LA conjugate due to ester bond formation. (c) Stacked Fourier transform-infrared (FT-IR) spectra of LA, TPGS, and TPGS-LA with a scanning range from 4000 to 500 cm^{-1} (d) UV−vis spectra of LA, TPGS, and TPGS-LA conjugate.

The FT-IR spectra of native TPGS shows a characteristic band at 1738.02 cm^{-1} which attributes to the carbonyl group (C-O) present in the TPGS. While comparing FT-IR spectra of LA with those of TPGS-LA, a shifting and strong absorption of the carbonyl band from 1707.30 to 1736.90 cm^{-1} was observed, confirming the replacement of the carboxyl group with the ester moiety, which thus provides evidence of ester bond formation between TPGS and LA.29 Additionally, peaks at 1143.60 and 2924.54 cm^{-1} correspond to -COO- and -CH_2 group stretching in TPGS, respectively (Figure 1c). UV−vis spectra of conjugate

were also recorded which reveal the appearance of both of the peaks corresponding to the λmax of both TPGS (λmax 280 nm) as well as LA (λmax 332).

The zebrafish is now a renowned model for assessing the biocompatibility of therapeutic agents because of its rapid and ex utero development which is ideally suited for the screening of potent molecules. Therefore, the biocompatibility of synthesized TPGS-LA conjugate was assessed in zebrafish embryos, and any maltransformations/lethality was observed until 120 hpf. The end point includes coagulation of embryos; loss of heartbeat; delayed hatching; deformation in the tail, eyes, and head; and reduced pigmentation. One distinctive aspect of zebrafish development is their sensitivity toward administered solutions in terms of timing and extent of hatching (which occurs around 2−3 dpf). Our results demonstrated that TPGS-LA conjugate imposed negligible variations in the morphology as well as the overall activity of larvae up to a 20 μM concentration (equivalent to LA; Figure 2).

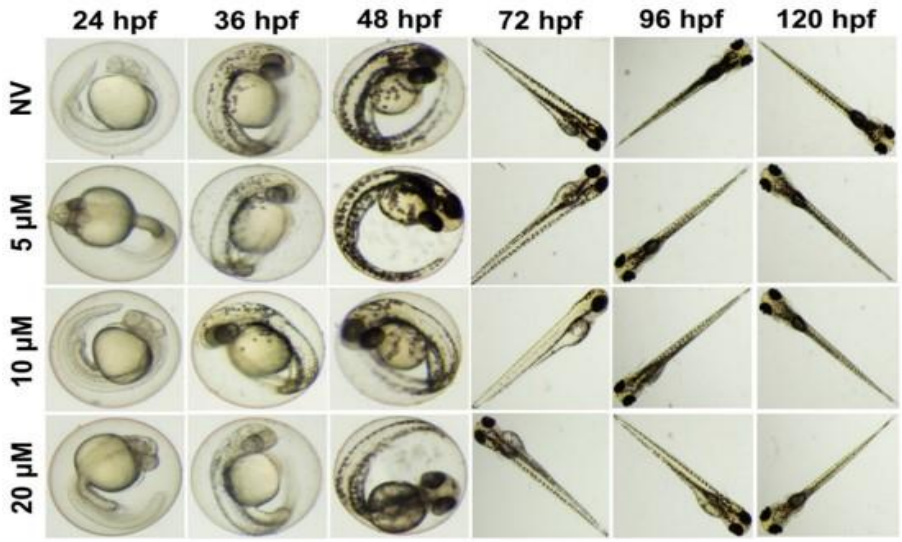

Figure 2: Photographic representation of the embryonic development of zebrafish upon treatments with different concentrations of TPGS-LA conjugate (5, 10, and 20 μM equivalent to LA) in system water over a period from 24 to 120 hpf.

PTZ is a chemical agent that causes seizures in animals by blocking the functioning of chloride channels via binding to the GABAA receptor. PTZ is considered to be a potent chemoconvulsant commonly used in the development

of experimental seizure models. Zebrafish larvae also behave identical to rodents when exposed to PTZ and exhibit concentration-dependent convulsing activity. Here, we have used an 8 mM concentration of PT which potentially induced a hyperactive response within the first few minutes of exposure followed by severe seizures to loss of posture as time passed. It has been established that the pretreatment of any antiepileptic compound or entity decreases the PTZ-induced hyperactive response and increases the time for the arrival of clonus-like seizures in the respective animal model. As seizures or convulsions are the most prominent and distinct symptom of epilepsy, latency in the arrival of clonus-like seizures was recorded to evaluate the pretreatment antiepileptic potential of synthesized TPGS-LA conjugate. Preincubated TPGS-LA conjugate (5 μM equivalent to LA) larvae and LA10 (10 μM) exhibited an increment in latency to PTZ-induced convulsions in comparison to PTZ and other LA groups (LA1 and LA5; Figure 3a). There was a significant ($p < 0.05$) increase in timing of clonus-like seizures in TPGS-LA conjugate (7.5 min) as compared to the PTZ group (4.1 min) and LA groups (LA1, 4.5 min; LA5, 4.9 min; and LA10, 5.53 min) whereas differences among LA1 and LA5 groups in comparison to the PTZ group were observed to be insignificant.

A significant increase ($p < 0.05$) in carbonylation of protein was observed in the PTZ-treated group of larvae in comparison to the naïve group. TPGS-LA-treated groups exhibited a marked decrease in protein carbonylation levels in comparison to PTZ (Figure 4a). However, no significant difference in protein carbonylation was observed between PTZ and LA10 groups. These results indicated that TPGS-LA at a 5 μM concentration significantly reduces the formation of carbonylated protein via reducing oxidative stress in comparison to the native LA at 10 μM.

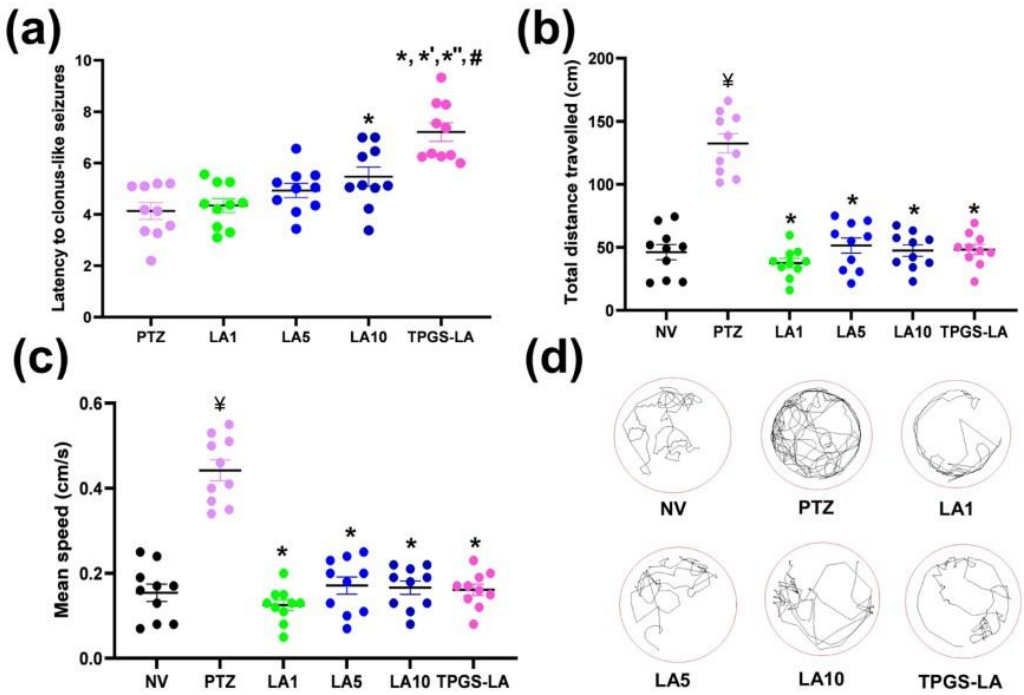

Figure 3: Effect of LA and TPGS-LA conjugate on (a) latency to clonus-like seizure and PTZ- induced hyperactivity as (b) total distance traveled in cm and (c) mean speed in cm/s. (d) Movement track of 7 dpf larva during PTZ exposure for 5 min. ¥ $p < 0.05$ as compared to NV, *$p < 0.05$ as compared to PTZ, *′ $p < 0.05$ as compared to LA1, *″$p < 0.05$ as compared LA5, and # $p < 0.05$ as compared LA10. NV: 7 dpf larvae incubated in system water, not exposed to PTZ. PTZ: system-water-incubated 7 dpf larva exposed to PTZ (8 mM). LA1: lipoic acid (1 µM)-incubated larva exposed to PTZ. LA5: lipoic acid (5 µM)-incubated larva exposed to PTZ. LA10: lipoic acid (10 µM)-incubated larva exposed to PTZ. TPGS-LA: TPGS-LA (equivalent to 5 µM lipoic acid)-incubated larva exposed to PTZ.

Our results are in corroboration with the earlier finding on PTZ-induced upregulation of *c-fos* expression in 7 dpf zebrafish larvae and also in rodent models. It is well-reported that PTZ exposure increases *c-fos* expression by several fold in different regions of the zebrafish larval brain, and the antiseizure entity reduces its expression. Altogether, our results demonstrated an ameliorated effect of TPGS-LA conjugate as compared to native LA in terms of latency in seizures, reduced hyperactivity, and downregulation of *c-fos* gene expression which are the markers of epilepsy, thus reflecting an enhanced

protective effect of TPGS-LA as compared to native LA in PTZ-induced convulsions.

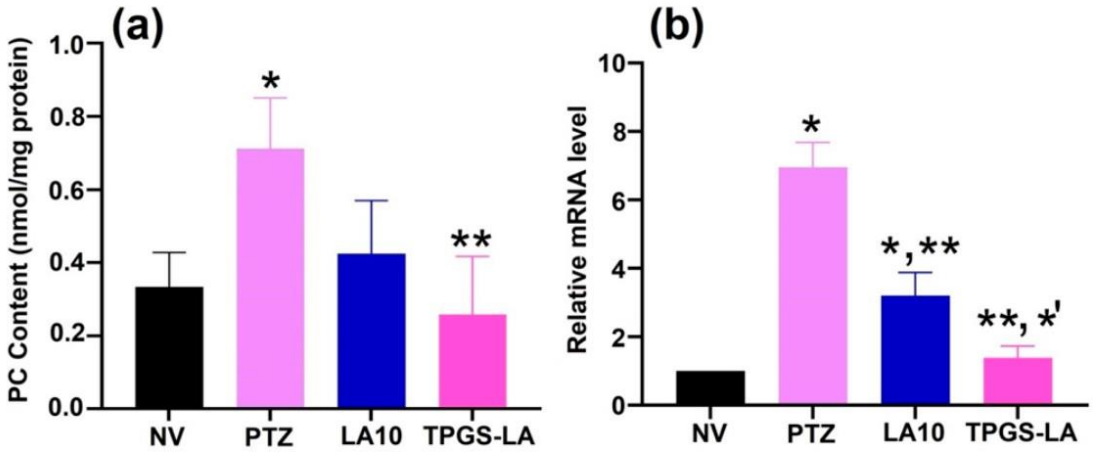

Figure 4: Effect of LA and TPGS-LA on (a) protein carbonylation levels in larvae exposed to PTZ and (b) c-fos expression of larvae exposed to PTZ. *$p < 0.05$ as compared to NV, **$p < 0.05$ as compared to PTZ, and *′$p < 0.05$ as compared to LA10. NV: 7 dpf larvae incubated in system water, not exposed to PTZ. PTZ: system water-incubated 7 dpf larva exposed to PTZ (8 mM). LA10: lipoic acid (10 µM)-incubated larva exposed to PTZ. TPGS-LA: TPGS-LA conjugate (5 µM)-incubated larva exposed to PTZ.

4.2 Development, Characterization and ameliorated anti-inflammatory efficacy of LA nanofiber

In this approach, PUL/LA/M-β-CD NF was developed by using one-step electrospinning technique, which offers the advantage of incorporating higher concentrations of cyclodextrin (23 % w/v) leading to encapsulation/solubilisation of higher amount of bioactive molecules. LA-M-β-CD IC was prepared by overnight incubation and then PUL (20 % w/v) was directly added to the inclusion complex solution resulting in the formation of clear and homogenous system. The viscosity and conductivity plays crucial role in the development and morphology of NFs, therefore, both parameters of electrospinning solution were recorded. The value of viscosity and conductivity of PUL/LA/ M-β-CD NF solution was determined as 1332 ± 12 mPa.s and 1.28 ± 0.008 S/cm, respectively. One-step electrospinning technique imparts the advantage of enhanced encapsulation of IC inside PUL NFs with entrapment efficiency of ~86.90 %. The PUL/LA/M-β-CD NF was successfully developed from electrospinning solutions and demonstrated

uniform, bead and defect free morphology with average NF diameter of 569 ± 129 nm (Figure 5c & d). This has been observed that low viscosity and high conductivity of the solution usually results in thinner fibres as compared to its counterpart. The deviation of PUL/LA/M-β-CD NF size from blank NFs (127 ± 23 nm; 1229.3 ± 50.2 mPa.s) may be due to encapsulation of LA-M-β-CD IC as well as increase in viscosity of PUL/LA/M-β-CD NF solution.

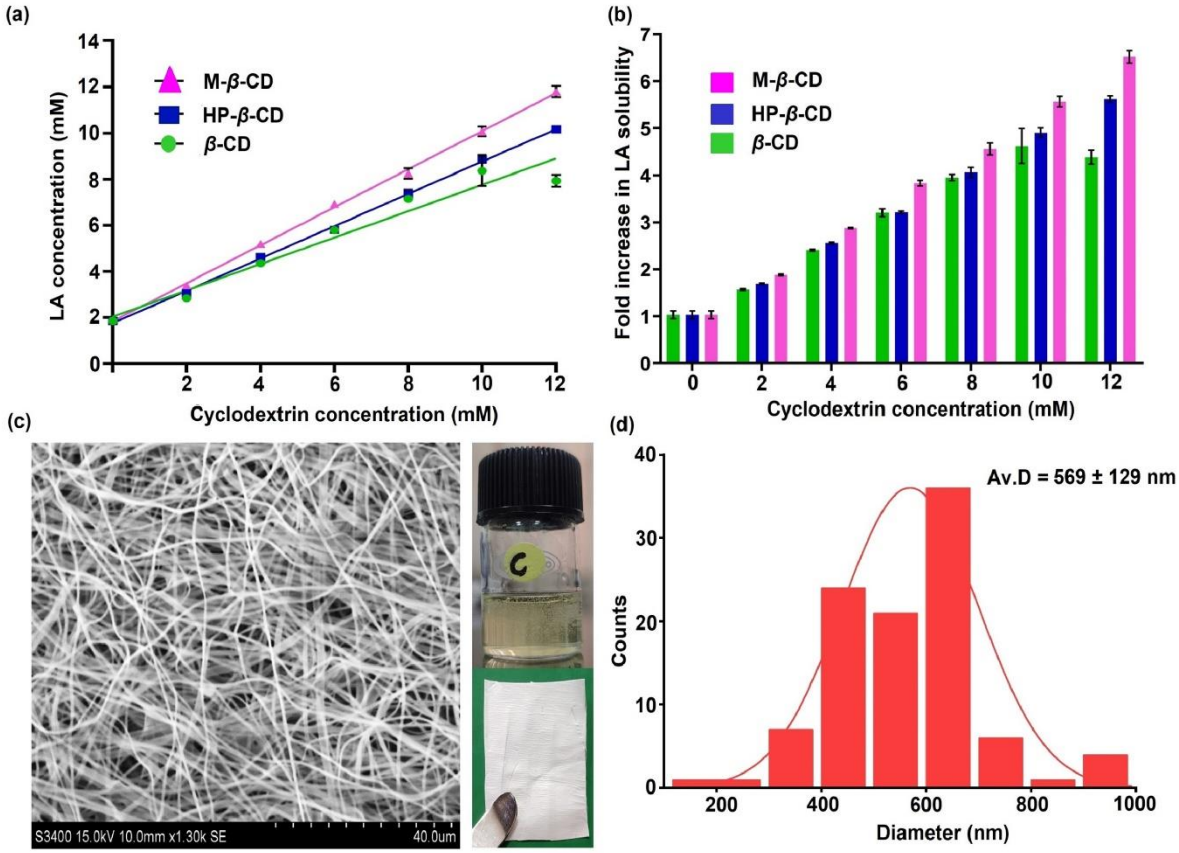

Figure 5: (a) Phase solubility curve and (b) fold increase in solubility of α-Lipoic acid (LA) with increasing molar concentration (0–12 mM) of β-CD (green colour); Hydroxypropyl- β-cyclodextrin (HP-β-CD; Navy blue colour) and Methyl-β-cyclodextrin (M-β-CD; magenta colour). (c) Scanning electron microscope image and (d) average fibre size distribution of PUL/LA/M-β-CD NF.

The presence and successful encapsulation of LA within PUL/LA/M□β-CD NFs were analysed by 1 H NMR spectra of LA, PUL, M-β-CD, and PUL/LA/M-β-CD NF individually. The distinctive peaks corresponding to the LA observed in the 1 H NMR spectra of the NF provided the evidence of LA being loaded into the

PUL/LA/M-β-CD NF (Figure 6) [2]. Notably, the characteristic peaks of LA in the spectra of both LA and PUL/LA/M-β-CD NF were identical, indicating the preservation of LA's chemical structure throughout the entire electrospinning process, thus ensuring its protection and stability [19,20].

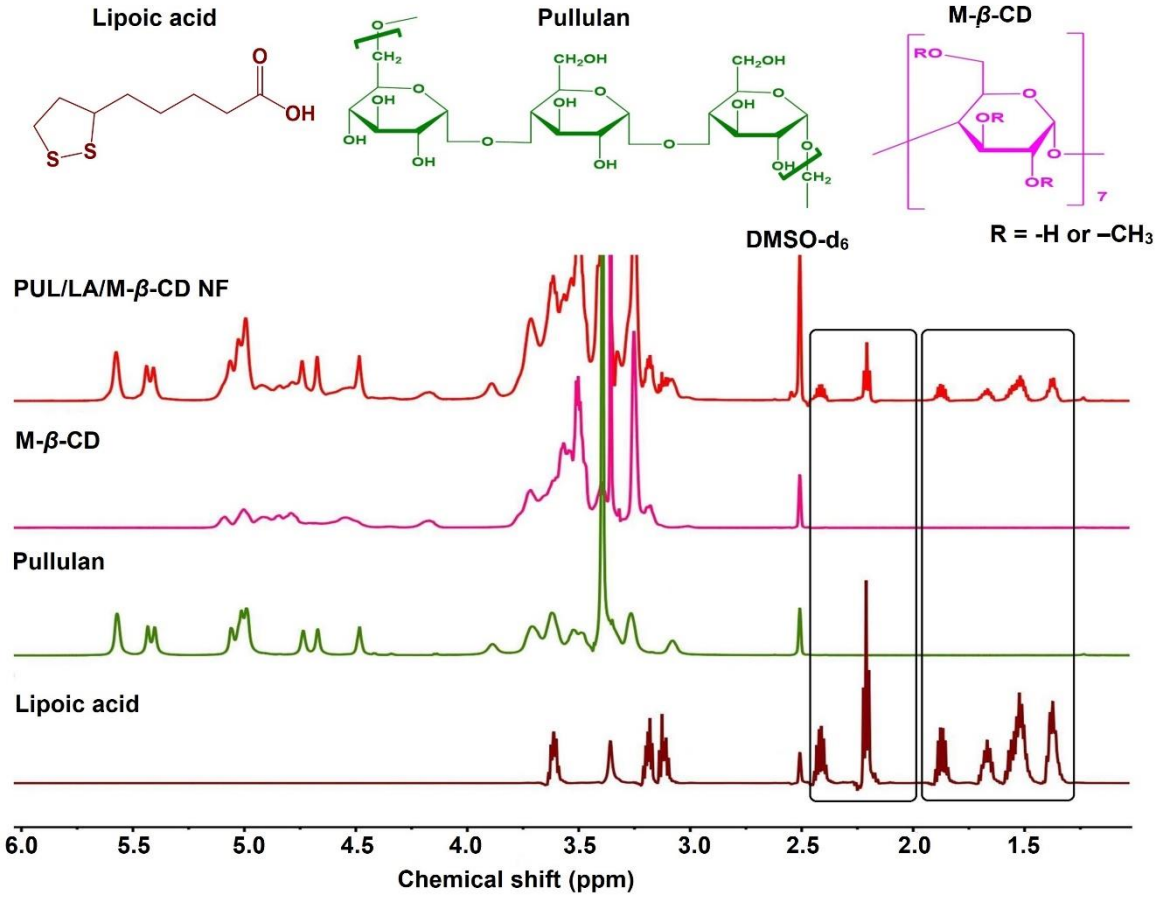

Figure 6: Proton NMR spectra of Lipoic acid (LA), Pullulan (PUL), Methyl-β-cyclodextrin (M-β-CD) and Pullulan/lipoic acid/M-β-CD nanofiber (PUL/LA/M-β-CD NF) in DMSO-d6 solvent. Highlighted portion represents the characteristic peaks of LA observed in both LA and PUL/LA/M-β-CD NF, indicating the successful encapsulation and preservation of LA during electrospinning process.

The cytocompatibility of developed PUL/LA/M-β-CD NF on RAW 264.7 cells was evaluated using MTT cell viability assay. The cell viability results demonstrated that PUL/LA/M-β-CD NF and LA has negligible effect on the viability of RAW 264.7 cells. Moreover, the induction of LPS (1 µg/mL) also demonstrated lesser to no influence on cell viability (Figure 7a and b). The effect of blank NFs on RAW

264.7 cells were also assessed and exhibited negligible effect on cell viability up to 500 µg/mL.

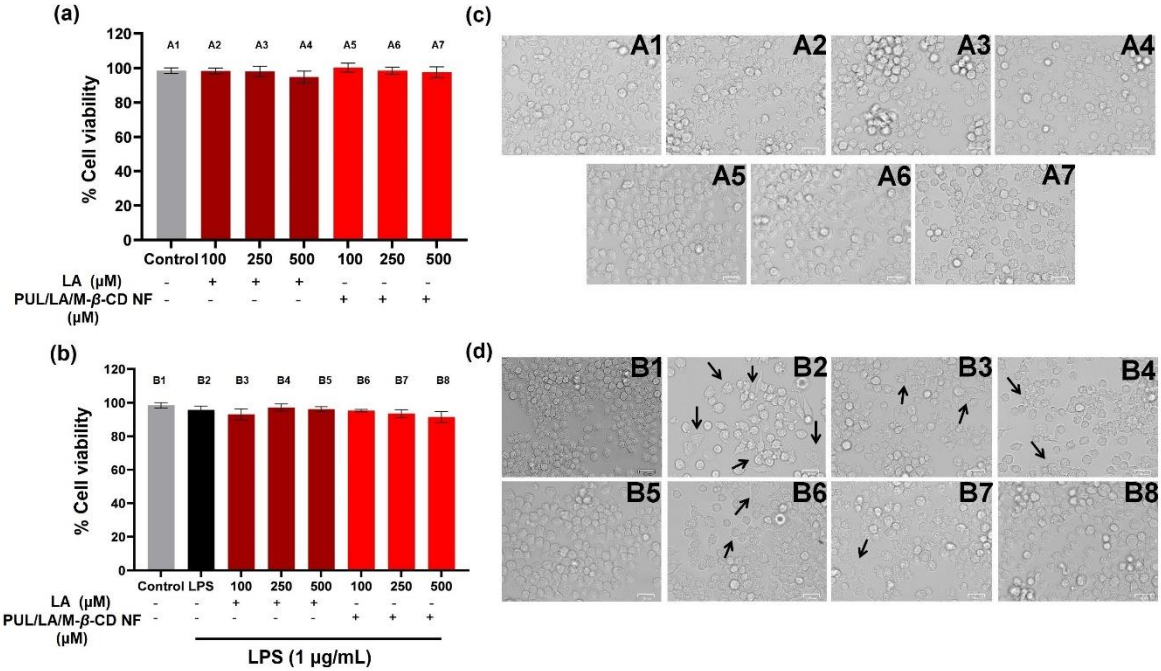

Figure 7: Effect of PUL/LA/M-β-CD NF on cell viability of RAW 264.7 cells in presence and absence of LPS induction. (a) & (b) cell viability graph of RAW 264.7 cells after 24 h treatment with LA and PUL/LA/M-β-CD NF at different concentration (100, 250 and 500 µM) without and with LPS, respectively. (c) & (d) microscopic images of RAW 264.7 cells representing morphological characteristics without (c) and with LPS induction (d). PUL/LA/M-β-CD NF demonstrated concentration□dependent retention of normal RAW 264.7 cells morphology even after LPS induction (B6, 7 &8). Black headed arrows indicate the morphological changes of macrophages after LPS induction. Images were captured using fluorescent microscope (ZOE™ Fluorescent Cell Imager, Bio-Rad). White line represents 25 µm scale bar.

NO, a pro-inflammatory mediator, is considered as a key marker of inflammation and is triggered by iNOS in macrophages. Its production is a part of the innate immune response in mammals and can indicate the progression of inflammation following exposure to LPS. However, excessive production of NO by triggered macrophages is associated with the development of inflammation-related disorders. Therefore, ameliorated effect of PUL/LA/M-β-CD NF on NO production in RAW 264.7 cells was evaluated using Griess reagent. The results

demonstrated significantly higher NO production in LPS group as compared to control group. However, PUL/LA/M-β-CD NF treatment demonstrated a significant concentration-dependent reduction in NO production compared to both LPS group as well as LA groups (Figure 8a).

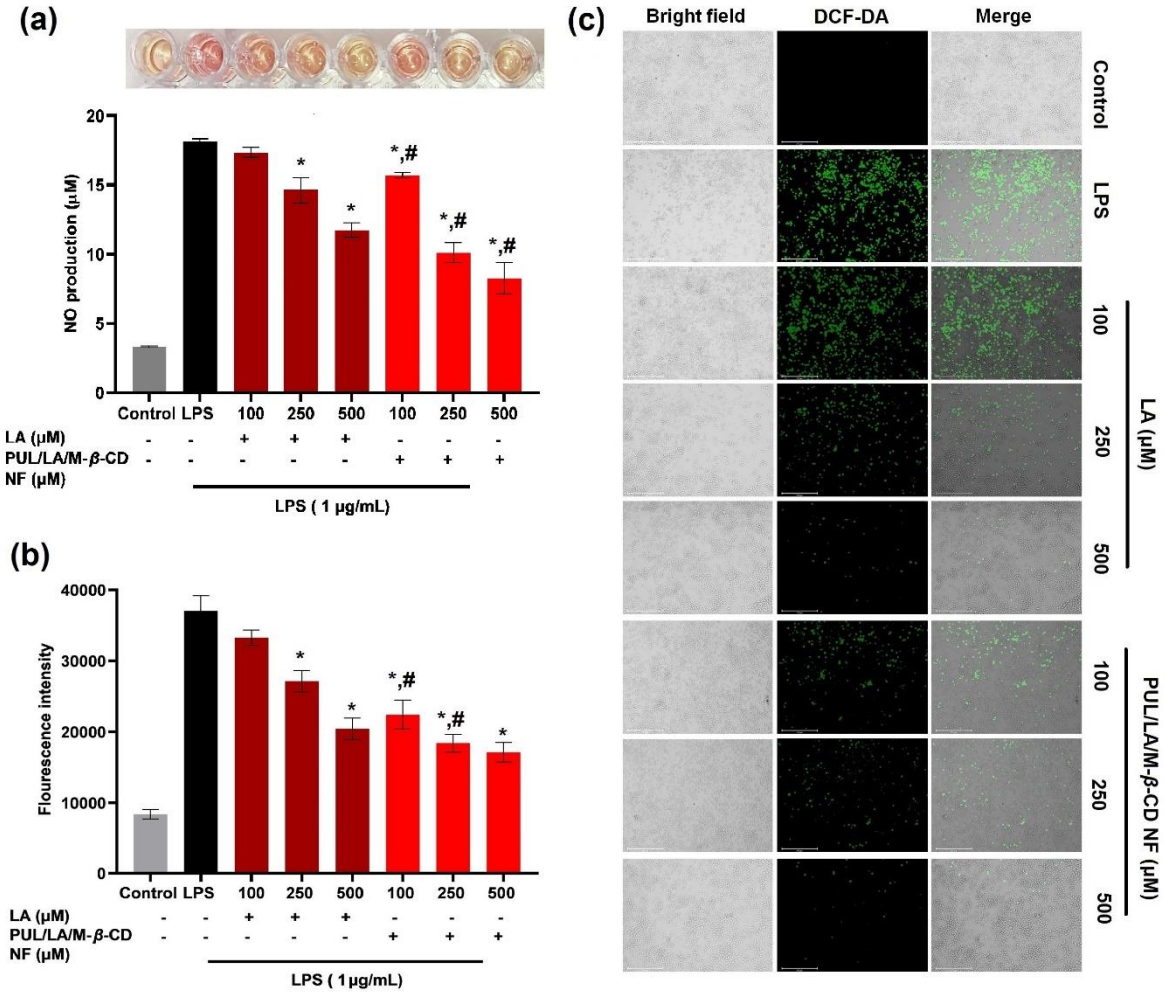

Figure 8: Effect of PUL/LA/M-β-CD NF on LPS induced NO and ROS production in RAW 264.7 cells after its 24 h treatment followed by 24 h LPS induction. (a) Graph of NO production in RAW 264.7 cells after 24 h treatment with LA and PUL/LA/M-β-CD NF at different concentrations (100, 250 and 500 μM) followed by LPS in□duction. PUL/LA/M-β-CD NF demonstrated concentration dependent ameliorated effect on LPS induced NO production. The amount of NO production was measured by Griess reagent. (b) Graph of ROS generation in RAW 264.7 cells after 24 h treatment with LA and PUL/LA/M-β-CD NF at different concentrations (100, 250 and 500 μM concentration) followed by LPS induction. Generation of ROS was evaluated by using DCF-DA fluorescent dye and change in fluorescence intensity was plotted as graph. (c) Microscopic images of ROS

generation, visualized using DCF-DA green fluorescent dye. Images were captured using fluorescent microscope (EVOS FL Auto 2 Cell Imaging System, Invitrogen). * $p < 0.05$ indicates significant difference in the mean value from LPS group. # $p < 0.05$ indicates significant difference in the mean value of PUL/LA/M-β-CD NF from LA group (with respective concentrations). White line represents 275 µm scale bar.

The results of ROS experiment demonstrated significant increase in ROS generation in RAW 264.7 cells upon induction of LPS as compared to the control group. However, PUL/LA/M-β-CD NF demonstrated a concentration-dependent decrease in ROS generation, which was more pronounced in comparison to both LPS and LA groups (Figure 8b). Microscopic images of ROS visualized using DCF-DA fluorescent dye also demonstrated the efficacy of PUL/LA/M-β-CD NF in significantly decreasing the ROS generation as compared to native LA.

The results of qRT-PCR demonstrated that PUL/LA/M-β-CD NF significantly downregulates the mRNA levels of iNOS, COX-2, TNF-α, IL-1β, and IL-6 compared to both LPS and LA (250 µM) group. Further, the results of COX-2 Western blotting demonstrated that PUL/LA/M-β-CD NF treatment significantly suppressed the protein expression of COX-2 in RAW 264.7 cells as compared to the LPS and LA group (250 µM concentration) (Figure 9c). Moreover, RAW 264.7 cells of control group presented negligible expression of COX-2 protein which is usually observed in LPS untreated cells whereas, a significant upregulation of COX-2 protein expression was observed in LPS group. we further assessed the ability of NF to suppress the nuclear translocation of NF-κB. The results demonstrated that PUL/ LA/M-β-CD NF (at 250 µM equivalent to LA) significantly suppresses the nuclear translocation of NF-κB in comparison to LA (Figure 10).

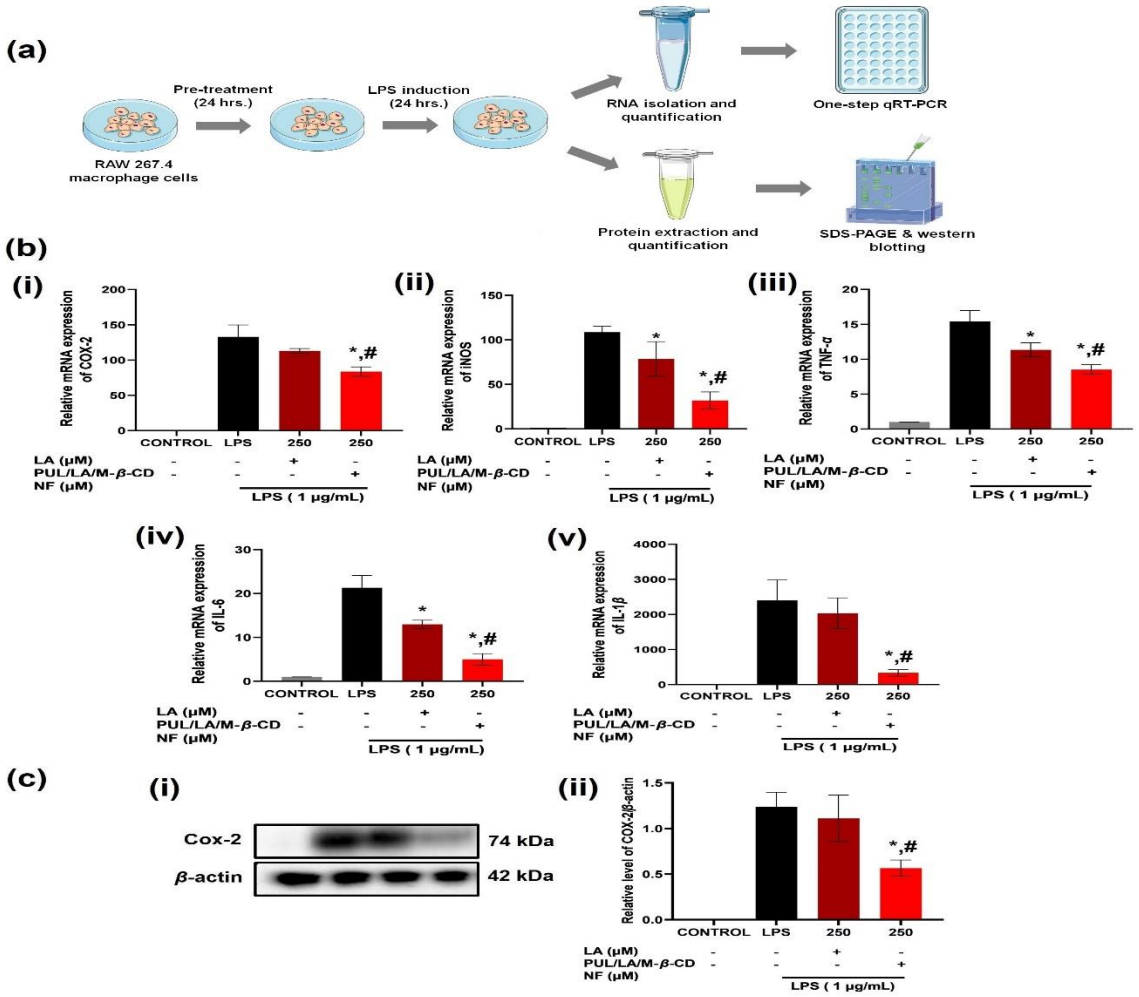

Figure 9: (a) Schematic representation of methodology followed for the treatment, protein and RNA isolation from LPS induced RAW 264.7 cells. (b) & (c) Suppressive effect of PUL/LA/M-β-CD NF on mRNA level of pro-inflammatory enzymes/cytokines and protein levels of COX-2 in LPS induced RAW 264.7 cells. mRNA levels of iNOS, COX-2, TNF-α, IL-6 and IL-1β was analysed by qRT-PCR in cells treated with LA and PUL/LA/M-β-CD NF (250 μM equivalent to LA) for 24 h followed by induction of LPS (1 μg/mL) for another 24 h. Protein expression of COX-2 was analysed by Western blotting in cells treated with LA and PUL/LA/M-β-CD NF (250 μM equivalent to LA) for 24 h followed by induction of LPS (1 μg/mL) for another 24 h. *p < 0.05 indicates significant difference in the mean value from LPS group. #p < 0.05 indicates significant difference in the mean value of PUL/LA/M-β-CD NF from LA group (with respective concentrations).

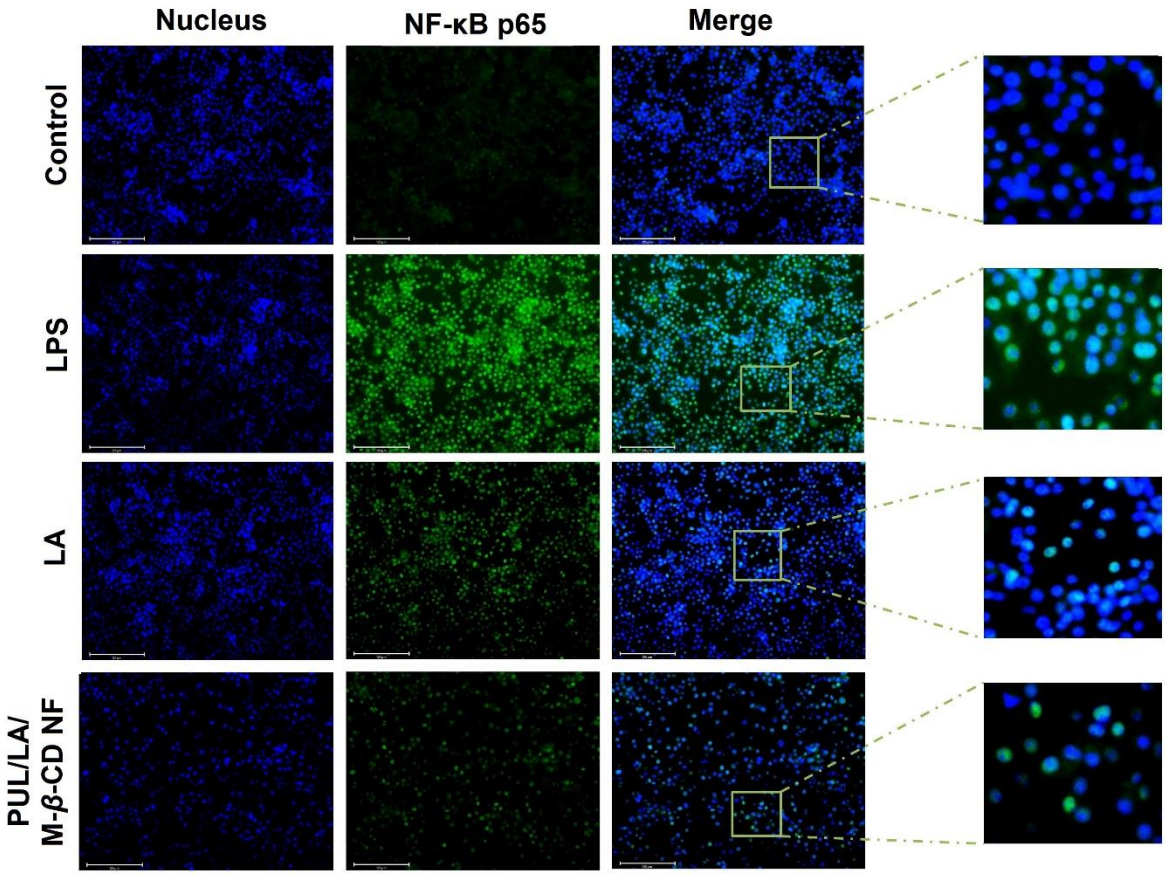

Figure 10: Inhibitory effect of PUL/LA/M-β-CD NF on LPS-stimulated nuclear translocation of NF-κB in RAW 264.7 cells analysed by fluorescent microscopy. Macrophages were immunostained by Alexa Fluor 488 for NF-κB and DAPI for nuclei staining. Images were captured using fluorescent microscope (EVOS FL Auto 2 Cell Imaging System, Invitrogen). White line represents 125 µm scale bar.

4.3 Development, Characterization and ameliorated anti-asthmatic efficacy of LA solid dispersion

Soluplus based solid dispersion of LA was prepared to improve the bioavailability of LA. The resulting solid dispersion has the appearance of a dry and fine powder (Figure 11). The encapsulation efficiency of LA-SD was analysed to be 100 % with maximum percent yield.

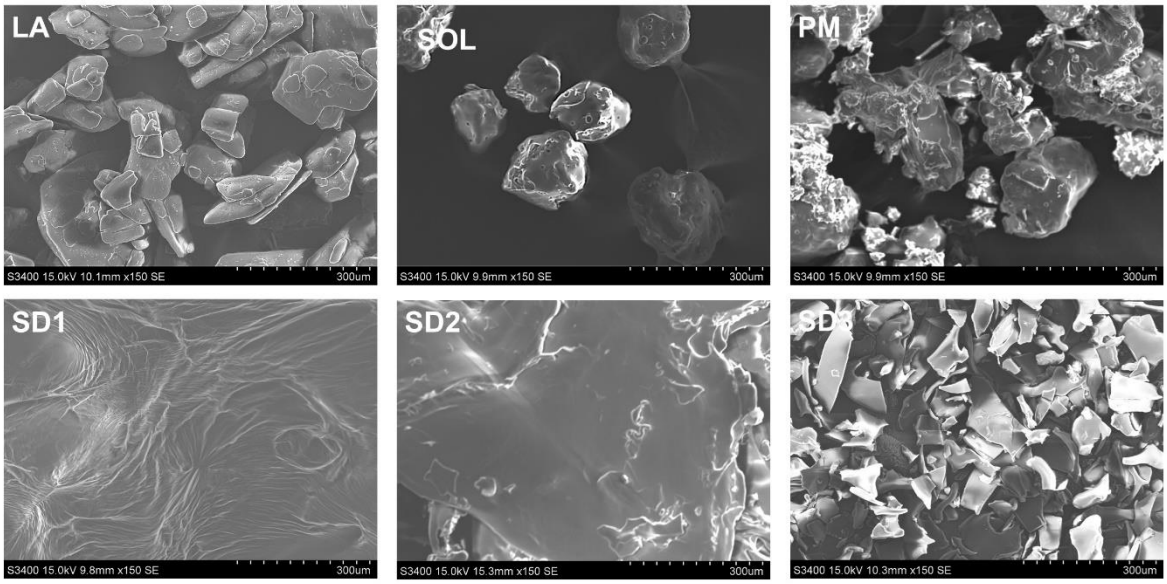

Figure 11: Scanning electron microscope image of LA, SOL, PM, SD1, SD2 and SD3 showing change on morphology of Lipoic acid after solid dispersion formation.

The FT-IR spectrum of LA, SOL and LA-SD was recorded to determine the possible molecular interaction between LA and SOL. The spectra of SOL exhibited characteristic peaks at 3549.47 cm^{-1}, 3471.99 cm^{-1}, 3418.59 cm^{-1}, 2930.83 cm^{-1}, 2858.76 cm^{-1} and 1618.27 cm^{-1} of hydroxyl, aliphatic acid carbonyl region **(Figure 12a)**[13]. In contrast to LA, no significant sharp band was observed in FTIR spectrum of LA-SD indicating successful encapsulation of LA inside polymeric carrier. Moreover, in LA-SD broadening of peak at 3400 cm^{-1} regions in comparison to extract may be due to possible hydrogen bonding interaction between both the components.

The thermograms of LA, SOL and LA-SD were obtained to gather their thermochemical information. A sharp endothermic peak at 60 °C observed in DSC thermogram of LA indicating its melting point and crystalline structure **(Figure 12b)**. No distinct peaks were observed in SOL over the entire range of temperatures detected indicating its amorphous nature which is also reported previously[13]. Similarly, no such endothermic peaks were seen in the thermogram of LA- SD, suggesting complete encapsulation of LA and dispersed molecularly in the amorphous SOL carrier.

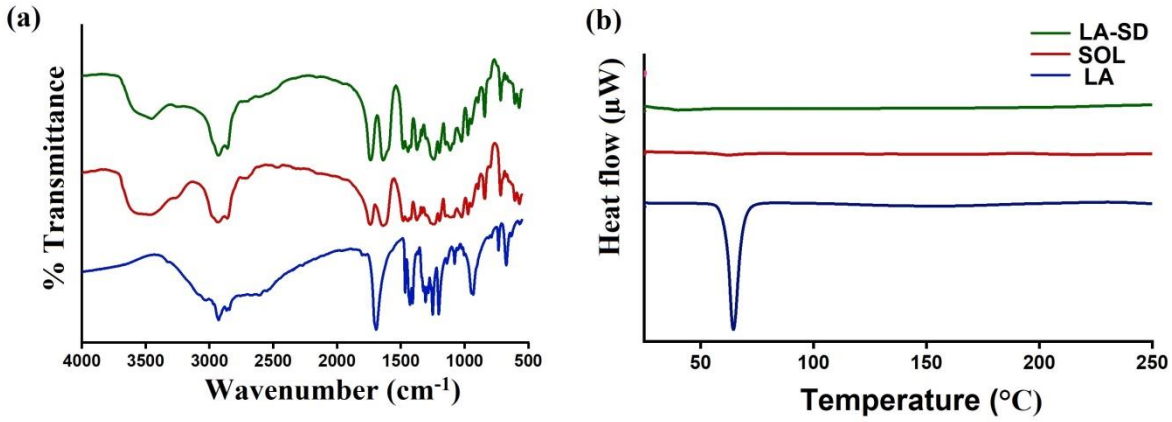

Figure 12: Solid state characterizations (a) FT-IR spectra, (b) DSC thermograms of native LA, Soluplus (SOL) and lipoic acid solid dispersion (LA-SD).

Further, the therapeutic efficacy of developed solid dispersion was evaluated in OVA-LPS induced allergic asthma murine model. Allergic asthma is a chronic inflammatory condition and one of the most widespread lung diseases globally. Biomolecules are increasingly recommended as a beneficial approach for treating inflammatory diseases, including asthma and COPD. The safety and affordability of natural medicines have led modern scientific research to focus on these remedies for respiratory conditions. The results of study demonstrated that developed LA sild dispersion significantly reduced the damage caused by OVA-LPS in murine model in comparison to diseased and LA group (Figure 13).

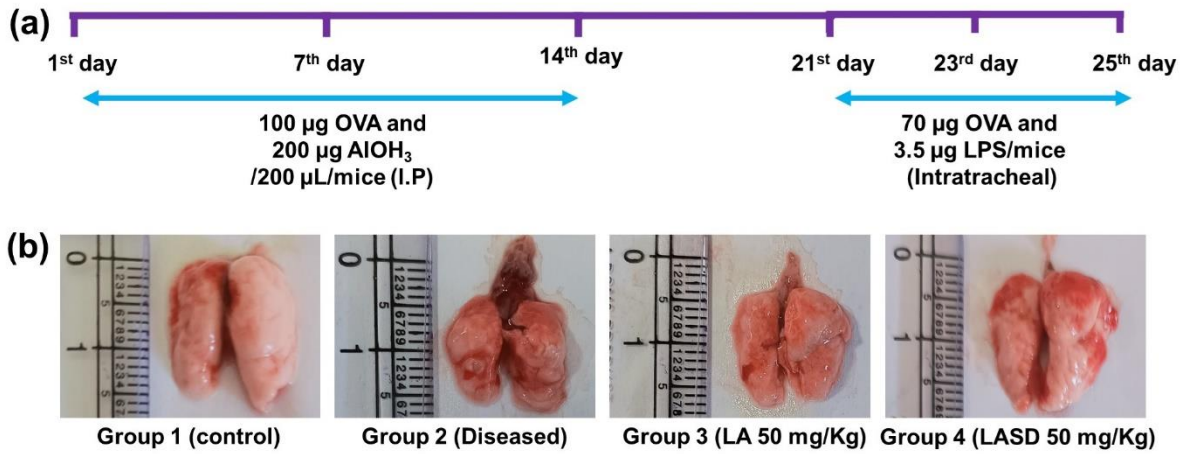

Figure 13: (a) Schematic study design for investigating effect of LA and LASD (50 mg/kg b.w.) in OVA-LPS-induced lung allergic inflammation. (b) Lungs images captured after dissection of the animals showing change in appearance of lungs before and after treatment.

5. Conclusion

In nutshell, the results of all three approaches, polymer-drug conjugation, cyclodextrin inclusion complexes combined with nanofiber technology, and solid dispersion techniques demonstrated very effective in ameliorating the solubility, dissolution and therapeutic efficacy in all possible preclinical *in vitro* as well *in vivo* animal models (zebrafish and murine).

6. Impact of the research in the advancement of knowledge or benefit to mankind

The research on α-Lipoic acid (LA) formulations holds significant clinical relevance, particularly in the treatment of a range of conditions including hepatic, cardiovascular, diabetic, and neurodegenerative diseases like Alzheimer's, as well as early infantile epileptic encephalopathy. LA's potent antioxidant properties, which allow it to neutralize free radicals, make it a promising therapeutic agent. However, its clinical application has been limited by challenges such as poor solubility, thermal instability, and low bioavailability.

This work represents a significant advancement in overcoming these barriers by exploring innovative formulation strategies: polymer-drug conjugation, cyclodextrin inclusion complexes with nanofiber technology, and solid dispersion techniques. These strategies not only enhance the bioavailability and stability of LA but also make it more effective in its therapeutic roles, particularly in the prevention and treatment of complex conditions like epilepsy and allergic asthma.

The successful development of these formulations could greatly benefit mankind by making LA-based treatments more accessible, effective, and patient-friendly. This has the potential to improve the quality of life for patients suffering from chronic and debilitating diseases, offering new hope in areas where current treatment options are limited or inadequate. By advancing the clinical application

of LA, this research could lead to more effective therapies, ultimately contributing to better healthcare outcomes on a global scale.

7. References

1. S.-y. Lv, S. He, X.-l. Ling, Y.-q. Wang, C. Huang, J.-r. Long, J.-q. Wang, Y. Qin, H. Wei, C.-Y. Yu, Review of lipoic acid: from a clinical therapeutic agent to various emerging biomaterials, Int. J. Pharm. (2022) 122201. https://doi.org/10.1016/j. ijpharm.2022.122201.
2. Ruchika, P. Kumari, D. Dhiman, A. Singh, Saneja, R-α-lipoic acid conjugated to d-α-tocopherol polyethylene glycol 1000 succinate: synthesis, characterization, and effect on antiseizure activity, J. Agric. Food Chem. 70 (25) (2022) 7674–7682, https://doi.org/10.1021/acs.jafc.2c01685.
3. D. Tibullo, G. Li Volti, C. Giallongo, S. Grasso, D. Tomassoni, C.D. Anfuso, G. Lupo, F. Amenta, R. Avola, V. Bramanti, Biochemical and clinical relevance of alpha lipoic acid: antioxidant and anti-inflammatory activity, molecular pathways and therapeutic potential, Inflamm. Res. 66 (2017) 947–959, https://doi.org/10.1007/ s00011-017-1079-6.
4. D. Kaur, T. Behl, A. Sehgal, S. Singh, N. Sharma, S. Chigurupati, A. Alhowail, A. Abdeen, S.F. Ibrahim, C. Vargas-De-La-Cruz, Decrypting the potential role of α-lipoic acid in Alzheimer's disease, Life Sci. 284 (2021) 119899, https://doi.org/ 10.1016/j.lfs.2021.119899.
5. N.V. Altunina, V.G. Lizogub, O.M. Bondarchuk, Alpha-lipoic acid as a means of influence on systemic inflammation in type 2 diabetes mellitus patients with prior myocardial infarction, J. Med. Life 13(1) (2020) 32. 10.25122/jml-2020-0018.
6. O. ¨ Çoban, S. Yıldırım, T. Bakır, Alpha-lipoic acid and cyanocobalamin co-loaded nanoemulsions: development, characterization, and evaluation of stability, J. Pharm. Innov. (2021) 1–11, https://doi.org/10.1007/s12247-020-09531-4.
7. A. Najafi, H.D. Kia, H. Hamishehkar, Does alpha-lipoic acid–loaded nanostructured lipid carriers improve post-thawed sperm quality and ameliorate apoptosis-related genes of rooster sperm? Poult. Sci. 100 (1) (2021) 357–365, https://doi.org/ 10.1016/j.psj.2020.10.007.

8. P. Gogoi, A. Dutta, A. Ramteke, T.K. Maji, Preparation, characterization and cytotoxic applications of curcumin-(±) α-lipoic acid coloaded phosphorylated chitosan nanoparticles in MDA MB 231 breast cancer cell line, Polym. Adv. Technol. 31 (11) (2020) 2827–2841, https://doi.org/10.1002/pat.5009.
9. S. Banik, S. Halder, H. Sato, S. Onoue, Self-emulsifying drug delivery system of (R)- α-lipoic acid to improve its stability and oral absorption, Biopharm. Drug Dispos. 42 (5) (2021) 226–233, https://doi.org/10.1002/bdd.2277.
10. Cao, N.; Feng, S.-S. Doxorubicin conjugated to d-α-tocopheryl polyethylene glycol 1000 succinate (TPGS): conjugation chemistry, characterization, in vitro and in vivo evaluation. Biomaterials 2008, 29 (28), 3856−3865.
11. Lu, C.; Kim, B. M.; Lee, D.; Lee, M. H.; Kim, J. H.; Pyo, H.-B.; Chai, K. Y. Synthesis of lipoic acid−peptide conjugates and their effect on collagen and melanogenesis. European journal of medicinal chemistry 2013, 69, 449−454.
12. L.M. Fonseca, C.E. dos Santos Cruxen, G.P. Bruni, A.M. ˆ Fiorentini, E. da Rosa Zavareze, L.-T. Lim, A.R.G. Dias, Development of antimicrobial and antioxidant electrospun soluble potato starch nanofibers loaded with carvacrol, Int. J. Biol. Macromol. 139 (2019) 1182–1190, https://doi.org/10.1016/j.
13. A. Celebioglu, T. Uyar, Encapsulation and stabilization of α-lipoic acid in cyclodextrin inclusion complex electrospun nanofibers: antioxidant and fast□dissolving α-lipoic acid/cyclodextrin nanofibrous webs, J. Agric. Food Chem. 67 (47) (2019) 13093–13107, https://doi.org/10.1021/acs.jafc.9b05580.
14. Fitriani L, Haqi A, Zaini E. Preparation and characterization of solid dispersion freeze-dried efavirenz–polyvinylpyrrolidone K-30. Journal of advanced pharmaceutical technology & research. 2016;7(3):105.
15. Sharma, P.; Kumari, S.; Sharma, J.; Purohit, R.; Singh, D. Hesperidin interacts with CREB-BDNF signaling pathway to suppress pentylenetetrazole-induced convulsions in zebrafish. Frontiers in pharmacology 2021, 11, 2178.
16. Bao, Y.; Guo, Y.; Zhuang, X.; Li, D.; Cheng, B.; Tan, S.; Zhang, Z. D-α-tocopherol polyethylene glycol succinate-based redox-sensitive paclitaxel prodrug for overcoming multidrug resistance in cancer cells. Mol. Pharmaceutics 2014, 11 (9), 3196−3209.
17. , Y.; Niu, B.; Song, Q.; Zhao, Y.; Bao, Y.; Tan, S.; Si, L.; Zhang, Z. RGD-decorated redox-responsive d-α-tocopherol polyethylene glycol

succinate−poly (lactide) nanoparticles for targeted drug delivery. J. Mater. Chem. B 2016, 4 (13), 2338−2350.

18. Saneja, A.; Sharma, L.; Dubey, R. D.; Mintoo, M. J.; Singh, A.; Kumar, A.; Sangwan, P. L.; Tasaduq, S. A.; Singh, G.; Mondhe, D. M. Synthesis, characterization and augmented anticancer potential of PEG-betulinic acid conjugate. Materials Science and Engineering: C 2017, 73, 616−626.
19. T. Alpha-lipoic acid−stearylamine conjugate□based solid lipid nanoparticles for tamoxifen delivery: formulation, optimization, in-vivo pharmacokinetic and hepatotoxicity study. J. Pharm. Pharmacol. 2016, 68 (12), 1535−1550.
20. Çoban, Ö .; Yıldırım, S.; Bakır, T. Alpha-Lipoic Acid and Cyanocobalamin Co-Loaded Nanoemulsions: Development, Charac□terization, and Evaluation of Stability. Journal of Pharmaceutical Innovation 2021, in press. DOI: 10.1007/s12247-020-09531-4.